Article

Estimation of the Friction Behaviour of Rubber on Wet Rough Road, and Its Application to Tyre Wet Skid Resistance, Using Numerical Simulation

Lingxin Zhang [1,2], Rongqian Wang [2,*], Haichao Zhou [1,2] and Guolin Wang [2]

[1] AEOLUS Tyre Co., Ltd., Jiaozuo 454003, China
[2] School of Automotive and Traffic Engineering, Jiangsu University, Zhenjiang 212013, China
[*] Correspondence: 17852032758@163.com

Abstract: Tyre wet skid resistance greatly affects vehicle safety, and it is dependent on the frictional behaviour at the tyre–road interface; however, the currently available numerical models, using the finite element method, either neglect the road roughness or obtain the rightness using expensive computed tomography scans, rendering them inefficient and complex. This study aims to present an estimation method of rubber slides on a rough road, to study tyre wet skid resistance. A three-dimensional rough road model was established, using the harmonic superposition method; the sealing effect of the water film on a wet road was modelled in terms of the pseudo-hydrodynamic bearing effect; the contact pressure, hysteresis friction, and water film hydrodynamic lift force were calculated. Subsequently, a friction model was established that accounted for the road surface morphology, tyre properties, sliding speed, and contact pressure. The accuracy of the friction model was experimentally validated, using the published experimental results. The friction model was then adopted, to conduct a study of the wet skid resistance of a 205/55R16 tyre with two different tread patterns. The simulation results were consistent with the experimental results of braking distance on a wet road. Finally, the effects of road roughness, tread rubber, load, and inflation pressure on wet skid resistance were carried out and analysed. The works in this paper have important significance and practical value for the development of high-performance tyres.

1. Introduction

Most traffic accidents are caused by tyres with insufficient grip, especially on wet roads [1,2]. In particular, all forces and moments are transmitted through the tyre from the vehicle to the road, and the grip performance of a tyre on a wet road depends primarily on the frictional behaviour at the region where the tyre contacts the road. Skid resistance is a key performance indicator of tyre grip, and is defined as the friction force that develops when a rolling tyre is prevented from sliding on the road [3–5]; a lower wet skid resistance increases the risk of accident. According to the Federal Highway Administration of the U.S. Department of Transportation, approximately 21% of vehicle crashes (1,235,000 each year) in the United States are related to weather, with a vast majority of them due to wet pavement or rainfall [6]. Wet skid resistance is lower on wet than on dry roads, because of the decrease in friction. As per the kinetic energy theorem, for any car (with constant mass) braking on the same wet road, greater friction entails greater braking deceleration and shorter braking distance: this, in turn, entails better tyre wet skid resistance. Thus, tyre wet skid resistance is conventionally evaluated in terms of the friction between the tyre and the road [7]. To improve automobile safety, the European Union has stipulated regulations governing the wet grip performance of tyres. The accurate evaluation of tyre wet skid resistance for various tyre structures, and under various pavement conditions, is of concern to policymakers and the tyre industry.

The tyre is the only part of the vehicle that has direct contact with the road; therefore, the tyre's wet skid resistance directly influences the vehicle's braking distance, thus greatly increasing the risk of accidents under wet weather conditions. Studies have demonstrated that a tyre's wet skid resistance is affected by several factors related to the pavement, the tyre, and the environment [8,9]. Because the depth of the tyre tread grooves reflects how much more water is channelled away from the region of contact, this depth directly affects tyre wet skid and hydroplaning performance. A vehicle travelling fast has a low skid resistance, because the tyres do not have sufficient time to channel water away from the region of contact. In general, pavement surface texture and tyre characteristics are key variables that determine frictional behaviour and, by extension, the skid resistance of tyre-rolling on a wet road [10,11].

Skid resistance can be used to explain the contribution of road surface characteristics to the development of friction at the tyre–road interface, and tyre friction force is the result of a complex interplay between two principal components of the contact force: adhesion and hysteresis, as illustrated in Figure 1 [12]. When a tyre compresses against the rough road surface, the hysteresis force, resulting from rubber deformation and the contribution of energy loss to the frictional force on the rubber, is much larger than that of the adhesion force. Coming into contact with the rough surface of the road, the valleys on the microscopically uneven surface of the rubber are filled with water (Figure 2), which results in a pool preventing the rubber from penetrating the road surface valleys [13]: this removes the valley contribution to the friction force, due to the lubricant effect of the water film on the rough wet road; in this situation, the friction force between the tyre and the road surface is much lower than on a dry road, which leads to tyre slip, owing to the poor grip [14].

Researchers have thus experimentally investigated the frictional behaviour of tyre rubber under wet conditions: Sabey [15] conducted a friction test of a spherical rubber block, and determined the relationship between contact pressure and the wet friction coefficient; Grosch [16] conducted a series of studies on the influence of various factors, such as temperature and speed, on the wet friction coefficient, and determined the main curve describing rubber anti-skid performance; Takino [17] tested the relationship between the viscoelasticity of the tread compound and the wet friction coefficient in a tyre braking test; Deleau [18] studied the frictional behaviour of rubber on wet glass, and uncovered the effects of sliding speed and load on the wet friction coefficient; and Zhao [19] conducted several laboratory experiments to determine a function describing the relationship between the water film thickness and the friction coefficient.
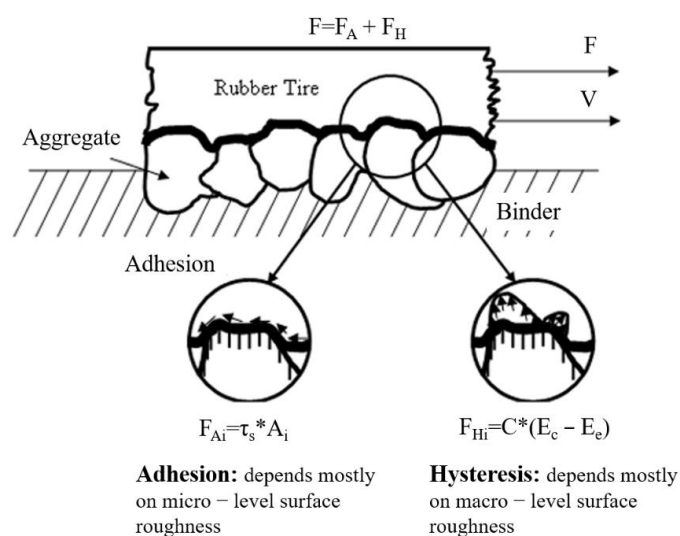

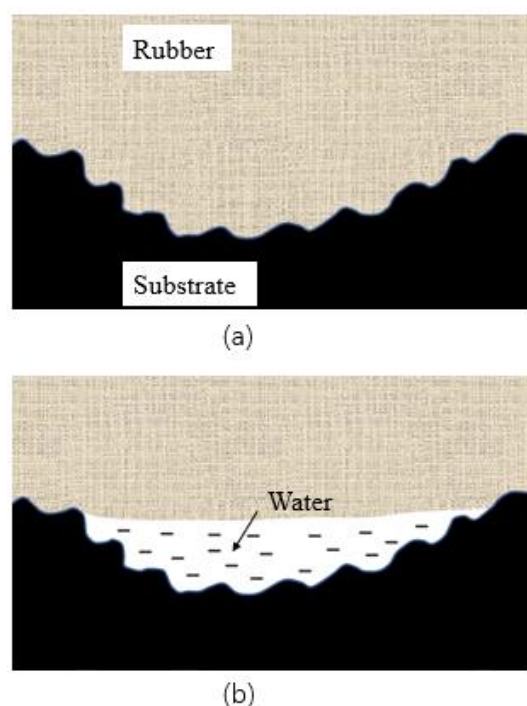**Figure 1.** Schematics of rubber contacting road.

Figure 2. Rubber sliding on rough road. (**a**) Dry road, (**b**) Wet road.

Tests allow researchers to investigate the frictional behaviour of the tread at the tyre–road interface; however, tyre performance tests are complex and expensive, often requiring expensive equipment and a long testing cycle, and they do not readily allow the researcher to account for tyre–road friction characteristics under slippery conditions. Thus, researchers have developed mathematical models of skid resistance with theoretical analysis. The models also allow for an analysis of the mechanisms. Greenwood [20,21] investigated the coefficient of the friction of spherical rubber bodies, and discovered that wet friction force mainly originates from hysteresis loss from rubber load deformation. Persson [22] calculated the wet friction coefficient of the tyre–road interface, by using the fractal friction theory of the road surface. With reference to the principle of conservation of energy, Ji [23] reported on the relationship of the wet friction coefficient to water film thickness and driving speed. Scaraggi [24] adopted the multiscale mean-field theory to investigate the lubricated contact between the tyre and a rough rigid surface, and discovered that the friction is greatly affected by the direction of the tread groove. Compared to using the experimental test, using the theory of physical properties for calculating the friction coefficient between the tyre and the wet road is more effective for revealing the influence of a single factor on the corresponding wet friction characteristics: however, these calculations are highly complex, and the parameters in the mathematical models are difficult to determine, resulting in relatively large errors in the calculation results.

Because those mathematical models require a large number of parameter combinations to analyse wet skid resistance, numerical simulation methods based on finite element theory can reflect the equivalent physical model of tyre wet skid resistance, and can be used to analyse the effects of different parameter combinations on wet skid resistance. Numerical simulation methods can be used not only for simulating tyre wet skid but also for obtaining force features, resulting in time and cost savings. Peng et al. [25] used a finite element simulation model to predict the maximum safe driving speed for a vehicle on a flat pavement in wet weather, and they determined the variations of the tyre–pavement friction coefficient with vehicle speed at different water film thicknesses [25]. Ding and Wang established a comprehensive three-dimensional (3D) grooved tyre–water–pavement interaction model, to predict hydroplaning speed on different pavement surfaces, and they noted that the tyre hydroplaning risk increases with the number of traffic lanes and the

presence of pavement rutting [26]. Tang et al. used a numerical tool to evaluate the wet skid resistance that accounted for the effects of pavement geometric design and tyre tread design, and they revealed the effects of pavement design parameters—for example, porosity and types—on the tyre wet skid resistance [27,28]; however, the pavement surface textures in Tang et al. were established through computed tomography (CT) scanning, which greatly limited the efficiency and practicability of the numerical simulation. Although road texture strongly affects rubber friction and tyre wet skid resistance, it was not fully accounted for in the aforementioned finite element simulation.

In summary, the aforementioned studies have elucidated the frictional behaviour of tyres on wet roads, and have aided the design of tyres with enhanced tyre wet skid resistance, but they have disregarded the roughness of the pavement and the effects of water sealing in the microscopic valleys of the road surface; furthermore, in existing models of the wet skid mechanism, the application of road roughness data obtained using CT scans has been limited. In this paper, a numerical method of modelling rubber friction on wet roads, to account for the influence of road roughness, is proposed. Tyre braking distance on a wet road was conducted, to verify the accuracy of the proposed friction model and simulation method.

2. Model of Frictional Behaviour for Rubber on Wet Rough Road

Models of tyre friction on a wet road must account for the effects of road roughness and water flume sealing. Figure 3 outlines the underlying framework of a friction model of tread rubber on a wet rough road. Specifically, a rough road is reconstructed using the road power spectrum density, and a model of sliding contact between the tread rubber and rough road is constructed to obtain the tyre rubber's vertical contact force and hysteresis force. Moreover, flume volume is calculated, with the effect of rubber sealing accounted for, and the water film hydrodynamic lift force is obtained, using the pseudo-hydrodynamic bearing effect. Subsequently, the friction coefficient of tread rubber on a wet rough road is calculated. Inspired by the exponential decay friction model, a friction model of tread rubber on a wet road, that accounted for contact pressure and sliding speed, was proposed. In addition, a tyre wet skid resistance simulation was conducted, to demonstrate the applicability of our proposed friction model.
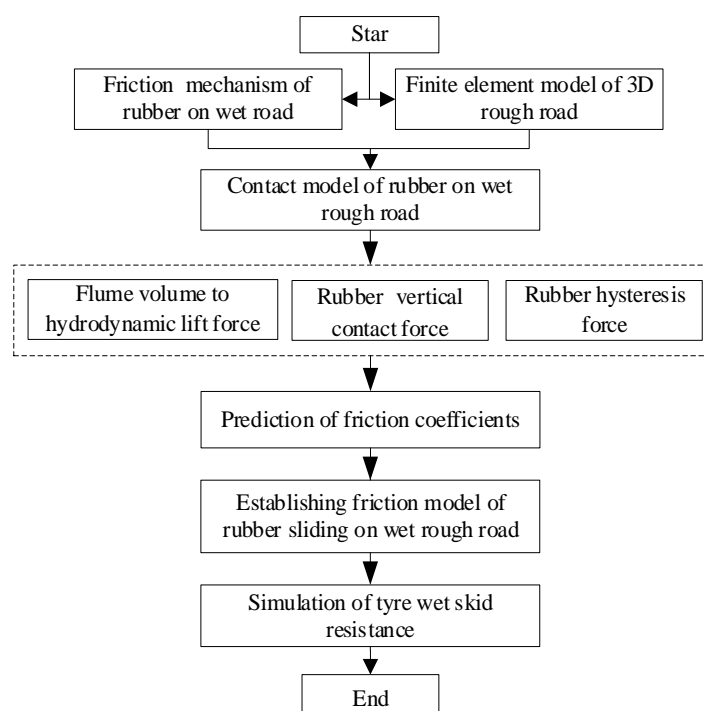

Figure 3. Framework of friction model.

2.1. Friction Mechanism of Tread Rubber on Wet Rough Road

Tyre–road friction has two main components: the first is adhesion friction, which is caused by the fracture and recombination of molecular bonds, and which occurs when the clean and smooth rubber surface comes into contact with the pavement; the second is hysteresis friction, which occurs when the tyre slides on a rough road. Hysteresis friction is caused by the energy loss of rubber viscoelasticity, which occurs because a different frequency of vibration is produced on the tread rubber, due to the road macro-texture. Frictional hysteresis is widely considered to be the more dominant component than frictional adhesion in rubber friction [29,30]. When a rolling tyre brakes on a wet rough road surface, the water film in the texture acts as a lubricant to prevent adhesion friction, and fills the microscopic valleys on the road surface, which generates a water sealing effect and a hydrodynamic lift force that hinders the contact between the tyre rubber and the road, thus reducing the rubber hysteresis friction. When modelling the interaction between a tyre and a wet rough road, the influence of hysteresis friction and water film hydrodynamic lift force on tyre wet skid resistance should be considered.

2.1.1. Hysteresis Friction

The hysteretic friction of viscoelastic rubber can be calculated using the viscoelastic–rough surface contact model proposed by Kane [3]. The contact model and forces distributions of the rubber block sliding on a rough road surface are illustrated in Figure 4. When the rubber block slides on the rough road, the hysteresis friction force can be calculated according to the asymmetry of the vertical contact force caused by the viscoelastic behaviour of the rubber. The control equation of the hysteresis friction force can be established, as written in Equation (1), according to the balance of forces in the directions of contact between the road surface profile and the slipping rubber block at a given moment; the governing equation in the contact zone is as follows:

$$\vec{F_i} + \vec{T_i} + \vec{R_i} + \vec{FR_i} = \vec{0} \tag{1}$$

where $\vec{F_i}$ is the vertical contact force of the rubber on the road surface, $\vec{T_i}$ is the traction force required to move the rubber, $\vec{R_i}$ is the normal force on the contact surface, $\vec{FR_i}$ is the local friction force, $\vec{FR_i} = \mu_{loc}\vec{R_i}$, and μ_{loc} is the local friction coefficient of the contact surfaces.

(**a**)   (**b**)
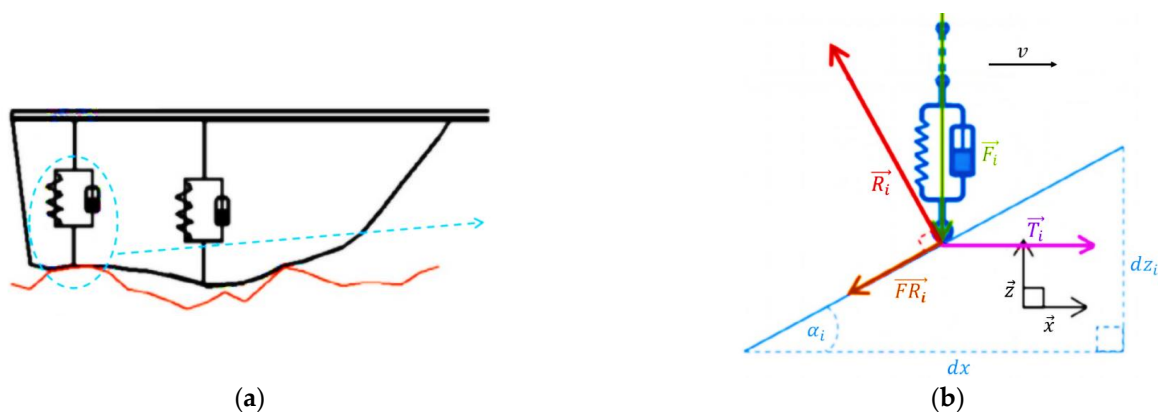
Figure 4. The sliding of a rubber block on a road surface: (**a**) deformed rubber in contact with a rough road; (**b**) forces acting on the contact surface.

By projecting Equation (1) onto the global *x*–*z* coordinates of the tyre–road interface, Equation (1) can be rewritten as follows:

$$\begin{cases} -F_i + R_i \cos(\alpha_i) - FR_i \sin(\alpha_i) = 0 \\ T_i - R_i \sin(\alpha_i) - FR_i \cos(\alpha_i) = 0 \end{cases} \tag{2}$$

When the rubber block is in contact with the road surface, the two-dimensional system couples the condition $\overrightarrow{FR}_{ij} = \mu_{loc}\overrightarrow{R}_{ij}$, as described in Equation (3):

$$T_i = F_i \frac{\sin(\alpha_i) + \mu_{loc}\cos(\alpha_i)}{\cos(\alpha_i) - \mu_{loc}\sin(\alpha_i)} \tag{3}$$

When the traction force is at the minimum required to move the rubber element, the traction force and the friction forces are almost equal, as described in Equation (4):

$$FF_i = T_i = F_i \frac{\sin(\alpha_i) + \mu_{loc}\cos(\alpha_i)}{\cos(\alpha_i) - \mu_{loc}\sin(\alpha_i)} \tag{4}$$

The total vertical load W applied on the rubber block can be balanced by the normal contact force, as described in Equation (5):

$$W = \sum_{i}^{N} F_i \tag{5}$$

Therefore, the global friction coefficient of the tread rubber on the road can be calculated using the following formula:

$$\mu = \frac{\sum_{i}^{N} FF_i}{W} \tag{6}$$

where W is the vertical contact force applied to the rubber block, and N represents the number of discrete rubber block elements.
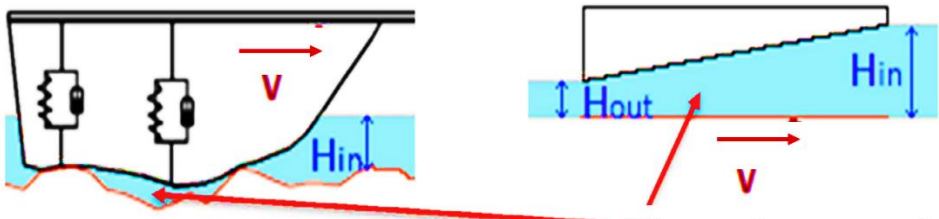
2.1.2. Hydrodynamic Effect of Water Film on Rough Road

When a tyre slides on a wet road, the water film fills the microscopic valleys in the road surface, which forms a flume, prompting a water sealing effect, and a hydrodynamic lift force is generated between the rubber and the road. The hydrodynamic lift force exerts a lifting force on the rubber from the road, and thus decreases the extent of the meshing of the microscopic peaks and valleys in the uneven road surface with those of the rubber surface: this decreases the contribution of hysteretic force to the frictional force of the rubber on the wet road, thus directly affecting the tyre's wet skid resistance. An extreme case is tyre hydroplaning, where the tyre has no contact with the road because of hydrodynamic effects. To account for the influence of hydrodynamic effects, Kane [3] converted the wet portion of the contact zone into a pseudo-hydrodynamic bearing with an equivalent continuous lubricant film, as shown in Figure 5. Kane then set the water volume of the pseudo-hydrodynamic bearing as equal to the water flume volume in the valleys of the rough road surface, and the hydrodynamic load could then be computed with the bearing load and subtracted from the load applied to the moving rigid pad. The hydrodynamic pressure P_h is calculated as follows:

$$\frac{d}{dx}\left(H(x)^3 \frac{dp_h(x)}{dx}\right) = 6\eta V \frac{dH(x)}{dx} \tag{7}$$

where $H(x)$ is the water film thickness at x in the bearing, η is the water viscosity, and V is the slip speed. The hydrodynamic lift force W_h is obtained through the hydrodynamic pressure integral to the tread rubber block. Subsequently, the total contact vertical force W_{total} and the wet friction coefficient μ_{wet} of the rubber block sliding on the wet road can be calculated, as written in Equations (8) and (9). Note that when $H_{in} = H_{out}$, the water film generates no hydrodynamic pressure, and also carries no vertical load; thus, the 'pseudo' hydrodynamic load capacity W_h is equal to zero.

$$\overrightarrow{W}_{total} = \overrightarrow{W} + \overrightarrow{W}_h \tag{8}$$

$$\mu_{wet} = \frac{\sum_i^N FF_i}{W_{total}} \qquad (9)$$

Figure 5. Diagram of rubber block contact with wet rough road.

2.2. Friction Model of Rubber on Wet Rough Road

2.2.1. Rough Road Model

Road surfaces deviate from an ideal (i.e., smooth and planar) surface, and their characteristics (e.g., surface texture, surface type, aggregate properties, and surface ageing) directly affect the frictional behaviour of tyres: a rougher road texture entails deeper microscopic valleys that can provide sufficient wet skid resistance for a fast-moving vehicle. Many studies have argued that road surface characteristics, especially road roughness, must be accounted for in a friction model [31]; therefore, road texture must be characterised, for an accurate and complete numerical analysis of tyre–road friction characteristics. In general, the measurement results of the profile of a road surface are random, and no specific expression can be obtained; however, the topography of the road surface (e.g., asphalt, cement, or granite pavements) is widely considered to exhibit self-affinity characteristics, and the power spectral density is conventionally used as an indicator for statistical descriptions of road texture features, as described in Equation (10):

$$G_q(n) = G_q(n_0)\left(\frac{n}{n_0}\right)^{-w} \qquad (10)$$

where $G_q(n_0)$ is the road roughness coefficient, n_0 is the reference space frequency 0.1 m^{-1}, and w is the frequency index 2. A lower $G_q(n_0)$ indicates a smoother road (and higher road level). Referring to the harmonic wave superposition method [32], the three-dimensional coordinates of a rough road model, with roughness coefficient $G_q(n_0) = 1.6 \times 10^{-5}$ m^3, were calculated using MATLAB software; subsequently, a three-dimensional (3D) road model was established, using the cubic interpolation function to smooth the three-dimensional coordinates, as shown in Figure 6.
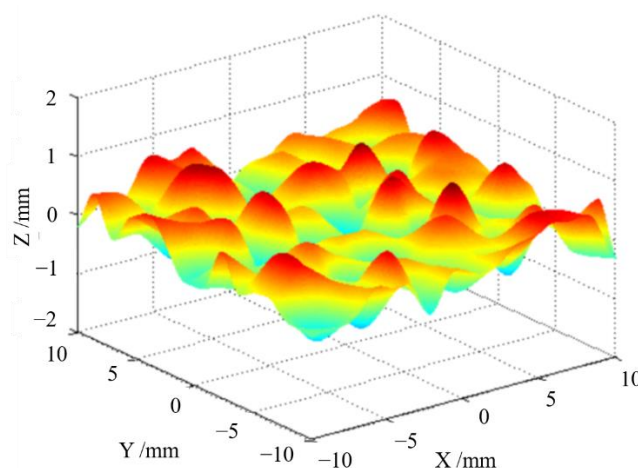

Figure 6. Coordinates of 3D road surface.

The 3D road profile in the model of the tyre–road interface was imported using the following steps: firstly, the three-dimensional coordinates of the asphalt pavement (Figure 6) were imported into the Digitized Shape Editor module of CATIA software, and mesh surfaces were generated using the software's mesh creation command; then, the automatic surface command was used, to fit the mesh surface that generated the 3D road surface; finally, the 3D solid model of the pavement was generated by extruding the road surface, and the extruded road model was cut, according to a plan, in the extruding direction, as illustrated in Figure 7a. The 3D solid road model was imported into HYPERMESH software, to generate the 3D finite element model of the road, as indicated in Figure 7b.
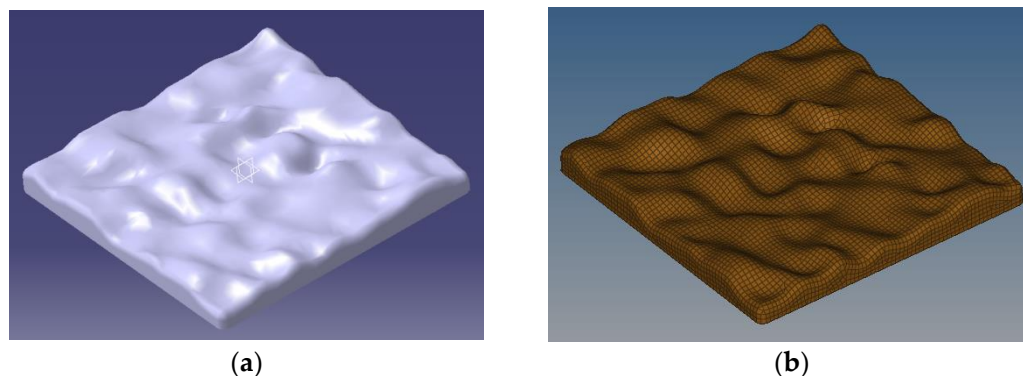

(a)   (b)

Figure 7. Reconstruction model of 3D road profile: (**a**) 3D road profile (**b**) mesh elements of 3D road model.

2.2.2. Contact Model of Rubber Sliding on a Rough Road

The contact model of the rubber block sliding on the 3D rough road was established in ABAQUS/Explicit solver, as shown in Figure 8, and the model parameters are detailed in Table 1. Because of differences in vertical stiffness, the rubber block was characterised in terms of viscoelastic behaviour, using a neo-Hookean hyperelasticity model and a Prony series model, and the road surface was assumed to be a discrete analytical rigid body. The parameters of the rubber block model are detailed in Table 2. To enhance contact interaction stability in cases of high-speed sliding, the boundary conditions of the contact model were determined according to the references [33,34]. Specifically, the top surface of the rubber block was set to be fixed with no sliding, and the velocity of the road was set to point on the y-axis, to represent the relative sliding motion between the rubber and the road. A vertical displacement in the z-axis applied on the road surface was used to generate contact pressure, and the contact force could be obtained by integrating contact pressure under different vertical displacements: this method has been widely applied in finite element analysis models of tyre behaviour [35].
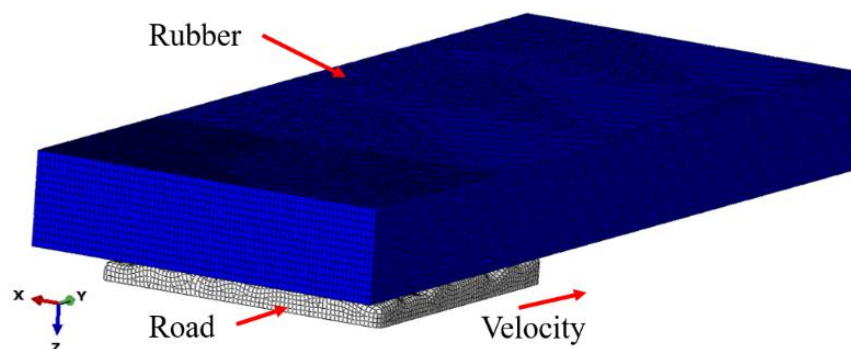

Figure 8. Contact model of tyre rubber sliding on a rough road.

Table 1. Finite element modelling parameters.

Part	Length/mm	Width/mm	Height/mm	Number of Elements	Element Type
Rubber	60	24	6	208,000	C3D8R
road	20	20	3	10,531	R3D3, R3D4

Table 2. Parameters of tyre rubber features.

Rubber Name	Neo-Hookean Model		Prony Model		
	C_{10}	D_1	$\bar{g}_1^p$	$\bar{k}_1^p$	$\bar{\tau}_1^p$
Rubber A	0.583	0.0346	0.1372	0	6.3211
Rubber B	0.671	0.03	0.1629	0	5.9846

Friction models differ greatly in how they describe the contact between the tyre and a dry road; in particular, compared with the coulomb friction model that maintains a stable friction force in a lager sliding ratio, the exponential decay friction model can not only more effectively capture the effects of sliding ratio and contact pressure on tyre friction, but also can describe the downward trend in frictional force over a larger sliding ratio range. The accuracy of the modelled downward trend was experimentally verified by Al-Qadi [36], and the friction coefficient is governed by the following equation:

$$\mu(p,v) = k \frac{\alpha \, p^d + \beta}{a + \frac{b}{v^{\frac{1}{m}}} + \frac{c}{v^{\frac{2}{m}}}} \left| \frac{E(f)}{1 - v^2} \right| \tag{11}$$

where v is the sliding speed; P is the contact pressure; a, b, c, d, and m are the fitting coefficients; k is the correction coefficient; v is the Poisson's ratio of the rubber; and $E(f)$ is the complex modulus of the rubber.

After the contact model was determined, the vertical contact force and hysteresis friction could be calculated, using numerical simulation. After the simulation process was completed, the contact model was imported into the HyperMesh software, to obtain the deformed rubber profile. Only the contact elements of the rubber surface interface with the road were retained, while the other elements were deleted. Subsequently, the coordinates of the contact elements were output. By assuming that the road surface valleys were filled with water film, and that the obtained volume of the road surface valleys under the rubber squeeze effect was equal to the water flume volume, then the water flume volume could be calculated, using the definite integral method of the coordinates in the MATLAB software. Considering the typical conditions of the tyres in Reference [28], the sliding velocities of the road were set as 3, 6, 9, 12, 15, and 18 m/s. The hysteresis friction forces and water flume volumes at different speeds and contact forces are presented in Table 3. As indicated in Table 3, at the same sliding speed, as the vertical contact force gradually increased, the hysteretic friction of the rubber also gradually increased, and the flume volume gradually decreased; furthermore, the ratio of the vertical contact force to the hysteresis friction force decreased with the vertical contact force at a constant sliding speed, and the change in ratio (where the frictional force decreased with the contact force) agreed well with the results obtained from experiments with the friction force test results [34].

Table 3. Simulation results of rubber sliding on a rough road.

	Sliding Speed 3 m/s					
Contact force/N	70.87	105.28	139.77	175.39	209.54	244.70
Hysteresis friction/N	76.46	108.74	138.22	164.18	190.44	213.23
'Flume' volume/mm^3	209.78	163.55	130.45	103.93	83.15	65.04

Table 3. *Cont.*

	Sliding speed 6 m/s					
Contact force/N	68.67	106.22	139.77	174.97	210.84	241.91
Hysteresis friction/N	67.88	100.00	125.96	150.61	175.44	193.65
'Flume' volume/mm^3	213.46	162.51	130.45	104.21	82.43	66.38
	Sliding speed 9 m/s					
Contact force/N	70.32	99.99	129.45	161.60	189.80	220.96
Hysteresis friction/N	64.26	88.92	111.07	132.92	151.51	170.48
'Flume' volume/mm^3	210.69	169.57	139.41	113.50	94.71	76.96
	Sliding speed 12 m/s					
Contact force/N	70.23	100.42	128.43	158.84	191.31	219.18
Hysteresis friction/N	60.79	83.80	103.89	124.72	144.73	163.15
'Flume' volume/mm^3	210.85	169.07	140.33	115.51	93.79	77.90
	Sliding speed 15 m/s					
Contact force/N	49.97	80.30	110.98	140.76	169.61	201.13
Hysteresis friction/N	43.17	66.19	90.07	110.78	128.04	145.90
'Flume' volume/mm^3	252.41	193.5	157.4	129.63	107.85	87.94
	Sliding speed 18 m/s					
Contact force/N	50.28	79.78	109.15	140.22	169.90	198.19
Hysteresis friction/N	42.73	64.73	86.06	106.44	125.98	142.97
'Flume' volume/mm^3	252.89	193.60	159.34	130.08	107.65	89.66

2.2.3. Friction Coefficient of Rubber on Wet Rough Road

When a rubber block slides on a wet rough road, the microscopic valleys in the road surface are filled with water that forms a flume, and a hydrodynamic lift from the water flume is generated, to support the rubber block: this reduces the frictional force, because water has a lower friction coefficient than does the road surface. In this study, the 2D pseudo-hydrodynamic bearing proposed by Kane [3] was extended to 3D space, to analyse the hydrodynamic lift from the water flume. According to the length and width of the road sample, a wedge-shaped fluid domain with a length and width of 20 mm × 20 mm was established (Figure 9).
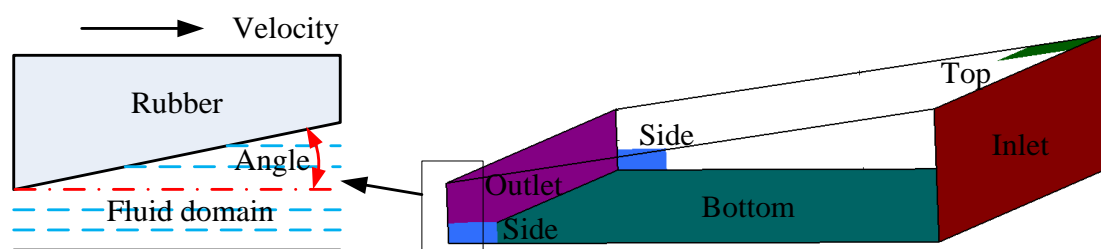

Figure 9. Fluid computational domain and boundary conditions.

A uniform velocity profile was applied at the inlet, according to the sliding speed. The outlet boundary condition was set as a pressure outlet, at a reference pressure of 0 Pa. No-slip wall boundary conditions were applied to the top, bottom, and two side surfaces of the computational domain. The flow field was initialised with a second-order-accuracy steady-state Reynolds-averaged Navier–Stokes equations (RANS) simulation, based on the Shear Stress Transport (SST) model. The numerical simulation was performed using the pressure-based solution available in ANSYS Fluent software (version 18.2). The Semi-Implicit Method for Pressure-Linked Equations Consistent (SIMPLEC) algorithm was selected to couple the pressure and velocity fields.

When the depth of the water outlet H_{out} is equal to the depth of the water inlet H_{in}, the water will support no load, and the water hydrodynamic lift is equal to 0. When the H_{out} is a constant value, the parameters H_{in} and β greatly influence the hydrodynamic lift when the volume of the water flume is fixed. The braking distances of a vehicle on dry and wet roads were tested separately on professional testing ground, and the results indicated that wet roads have a 25% smaller friction coefficient than do dry roads (Figure 10). Persson also reported that the frictional coefficient on wet surfaces is typically 20–30% smaller than that on dry surfaces [13]; therefore, it is assumed that a wet road has a 20–30% smaller friction coefficient than a dry road, and this determines the effect of the wedge angle β on the hydrodynamic lift.
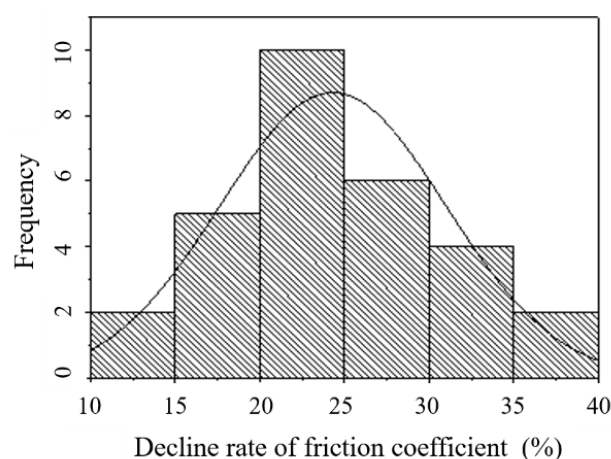

Figure 10. Frequency distribution of decline rate of friction coefficient.

To determine the wedge angle β of the fluid domain illustrated in Figure 6, the decline rate *Q* of the friction coefficient can be obtained from the following equations:

$$\mu_{wet} \approx \frac{\mu_{dry} F_{road}}{F_{road} + F_{water}} \tag{12}$$

$$Q = \frac{\mu_{dry} - \mu_{wet}}{\mu_{dry}} = 1 - \frac{\mu_{wet}}{\mu_{dry}} = 1 - \frac{F_{road}}{F_{road} + F_{water}} \tag{13}$$

where μ_{dry} and μ_{wet} are dry and wet friction coefficients, respectively, and F_{road} and F_{water} are the rubber contact force and water film hydrodynamic lift, respectively.

The effect of the wedge angle β on *Q* under different vertical contact forces (50.28 N, 109.15 N, and 198.19 N) and a constant sliding speed of 18 m/s was analysed, and the results are presented in Table 4. As indicated in Table 4, *Q* increased with β at a constant vertical contact force; however, when β was 0.4°, *Q* was about 25%, which was in the aforementioned range of 20–30%. Thus, β was set to 0.4°.

Table 4. Decline rate of friction coefficient with different wedge angles.

Contact force 50.28 N and Flume volume 252.89 mm³							
Wedge angle/°	0.1	0.2	0.3	0.4	0.5	0.6	0.7
hydrodynamic lift force/N	8.61	11.31	14.40	18.03	22.20	26.99	32.51
decline rate/%	14.62	18.36	22.26	26.39	30.63	34.93	39.27
Contact force 109.15 N and Flume volume 159.34 mm³							
Wedge angle/°	0.1	0.2	0.3	0.4	0.5	0.6	0.7
hydrodynamic lift force/N	13.76	18.67	24.90	32.53	42.19	54.50	69.95
decline rate/%	11.19	14.61	18.58	22.96	27.88	33.30	39.05

Table 4. *Cont.*

Contact force 198.19 N and Flume volume 89.66 mm^3							
Wedge angle/°	0.1	0.2	0.3	0.4	0.5	0.6	0.7
hydrodynamic lift force/N	22.04	31.68	46.90	68.86	104.03	160.16	247.56
decline rate/%	10.01	13.78	19.14	25.79	34.42	44.69	55.54

Subsequently, H_{in} and H_{out} were obtained at a fixed water flume volume, where $\tan(\beta) = (H_{in} - H_{out})/20$. As indicated in Table 5, the water hydrodynamic lift was negatively and positively correlated with the water flume volume and sliding speed, respectively.

Table 5. Calculation results of water hydrodynamic lift.

Sliding speed 3 m/s						
Flume volume/mm^3	209.78	163.55	130.45	103.93	83.15	65.04
hydrodynamic lift force/N	1.32	1.90	2.63	3.54	4.54	5.70
Sliding speed 6 m/s						
Flume volume/mm^3	213.46	162.51	130.45	104.21	82.43	66.38
hydrodynamic lift force/N	3.03	4.40	6.12	8.41	11.26	14.15
Sliding speed 9 m/s						
Flume volume/mm^3	210.69	169.57	139.41	113.5	94.71	76.96
hydrodynamic lift force/N	6.41	8.69	11.57	15.38	19.28	24.16
Sliding speed 12 m/s						
Flume volume/mm^3	210.85	169.07	140.33	115.51	93.79	77.9
hydrodynamic lift force/N	10.69	14.51	19.00	24.85	32.16	39.28
Sliding speed 15 m/s						
Flume volume/mm^3	252.41	193.50	157.4	129.63	107.85	87.94
hydrodynamic lift force/N	12.98	17.87	23.93	31.49	40.12	50.95
Sliding speed 18 m/s						
Flume volume/mm^3	252.89	193.60	159.34	130.08	107.65	89.66
hydrodynamic lift force/N	18.03	24.75	32.53	43.30	55.52	68.86

The equation for calculating the friction coefficient of rubber on wet road was derived from Equations (8) and (9), as follows:

$$\vec{F}_{total} = \vec{F}_{road} + \vec{F}_{water} \tag{14}$$

$$\mu_{wet} = \frac{F_{hys}}{F_{total}} \tag{15}$$

where F_{hys} is the hysteresis friction; F_{total} is the total vertical contact force; and F_{road} and F_{water} are the vertical contact force and the water hydrodynamic lift force, respectively. By feeding the hysteresis friction, vertical contact force, and hydrodynamic lift force values listed in Tables 4 and 5 into Equations (14) and (15), the friction coefficient of rubber on a wet rough road under different sliding speeds and contact forces can be calculated.

Two road types were used to analyse the change in the friction coefficient of rubber on dry and wet roads. The two road types were denoted A and B, and had roughness coefficients of $G_q(n_0) = 1.6 \times 10^{-5}$ and $G_q(n_0) = 25.6 \times 10^{-5}$, respectively. Figure 11 illustrates the changes in friction coefficients for sliding speed for different road types under a contact pressure of 0.3 MPa. The results indicated that the wet roads had a 1.4–21.0% lower friction coefficient relative to the dry roads, and that the friction coefficient was much lower at higher sliding speeds. These results agree well with those of [22,28], except for the magnitude of decrease: this difference may be attributable to differences in

the rubber material and the road surface texture. The results also indicated that rougher roads had higher friction coefficients. Of the dry roads, the friction coefficient of road B was larger than that of road A by 4–10%; of the wet roads, the friction coefficient of road A decreased by 2–26%, whereas the friction coefficient of road B decreased by 1.4–21% relative to the values for the dry roads: thus, an increased sliding speed corresponded to a smoother road and a greater decrease in the friction coefficient.
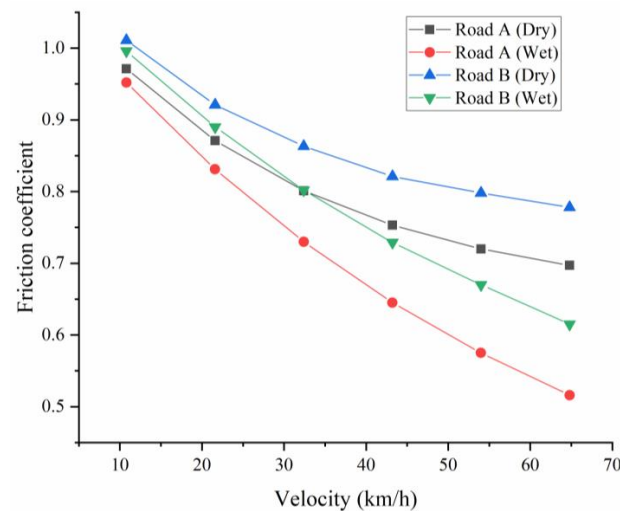
Figure 11. Friction coefficients in relation to sliding speed for different road types at a contact pressure of 0.3 MPa.

To determine why the road surface influenced the change of the friction coefficient, the actual contact features of roads A and B were obtained, as shown in Figure 12. The results indicated that when the rubber slid on wet road A and on wet road B, the rubber blocks failed to make complete contact with the valleys in the road surface. For the wet roads, the gaps between the rubber and the valleys were filled with water, and a water flume was generated. Because of the deformation of the rubber due to the contact force, the frictional force applied to the peaks of the road surface was asymmetrically distributed, being mainly concentrated in regions along the opposite direction of the sliding direction. Calculations indicated contact forces of 88.2 and 93.2 N, water film hydrodynamic lift forces of 34.0 and 27.8 N, and tyre contact areas of 108.7 and 118.2 mm^2 for roads A and B, respectively: that is, on a wet road, when the rubber was sliding on the rougher road B, the road bulge texture penetrated the rubber more easily, resulting in greater hysteresis friction and a friction coefficient that was less affected by the water flume hydrodynamic lift. Thus, it can be inferred that tyre wet skid resistance is improved on rougher roads, because the influences of the water film sealing effect and the water film hydrodynamic lift are weaker.
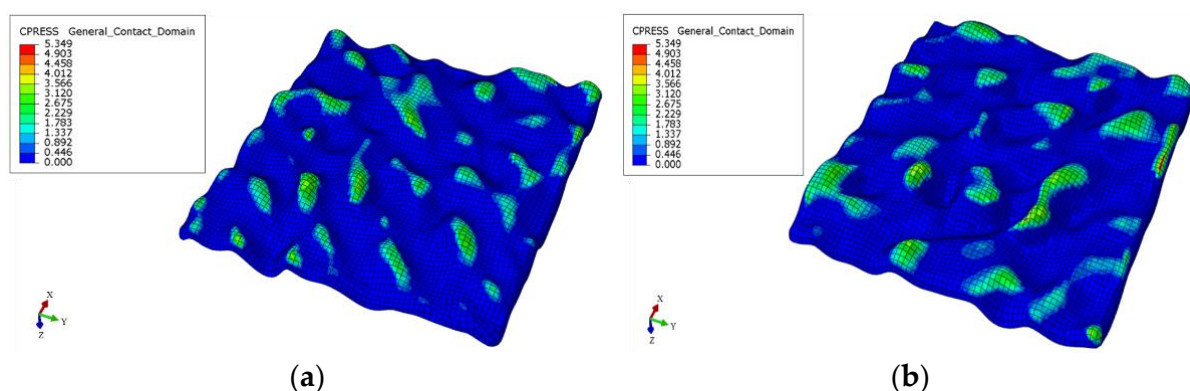

Figure 12. Contact pressure distribution of rubber on road A and B: (**a**) road A; (**b**) road B.

2.2.4. Friction Model of Rubber on Wet Road

When a tyre slides on a wet road, the friction behaviour in the contact zone changes with the distribution of the contact pressure and the sliding speed. According to the aforementioned simulation results, and to characterise the friction behaviour of the tyre contact with the wet road under different contact pressures and sliding speeds, an extended exponential decay friction model that accounted for the effect of contact pressure on model parameters was established. The model was based on the exponential decay friction model proposed by Oden [37], as described in the following equations:

$$\mu(v) = \mu_k + (\mu_s - \mu_k)\exp(-d_c v) \tag{16}$$

$$\begin{bmatrix} \mu_k \\ \mu_s \\ d_c \end{bmatrix} = \begin{bmatrix} \alpha_0\ \alpha_1\ \alpha_2 \\ \beta_0\ \beta_1\ \beta_2 \\ \gamma_0\ \gamma_1\ \gamma_2 \end{bmatrix} \begin{bmatrix} 1 \\ p \\ p^2 \end{bmatrix} \tag{17}$$

where u_k is the dynamic friction coefficient, u_s is the static friction coefficient, v is the sliding speed, and d_c is the decay coefficient. $\alpha_0 \sim \alpha_2$, $\beta_0 \sim \beta_2$, and $\gamma_0 \sim \gamma_2$ are nine fitting parameters related to the contact pressure P.

The nonlinear least squares method was used to fit the model parameters of Equation (16); the fitting parameters are listed in Table 6. The fitting curves of wet friction coefficients for different roads under different contact pressure are illustrated in Figure 13; the fitting results accurately reflected the relationship of the friction coefficient to the contact pressure and sliding speed. After the model parameters were obtained, Equation (16) could be plugged into Abaqus software as a user subroutine, to simulate tyre wet skid resistance.

Table 6. Fitting results for friction model parameters.

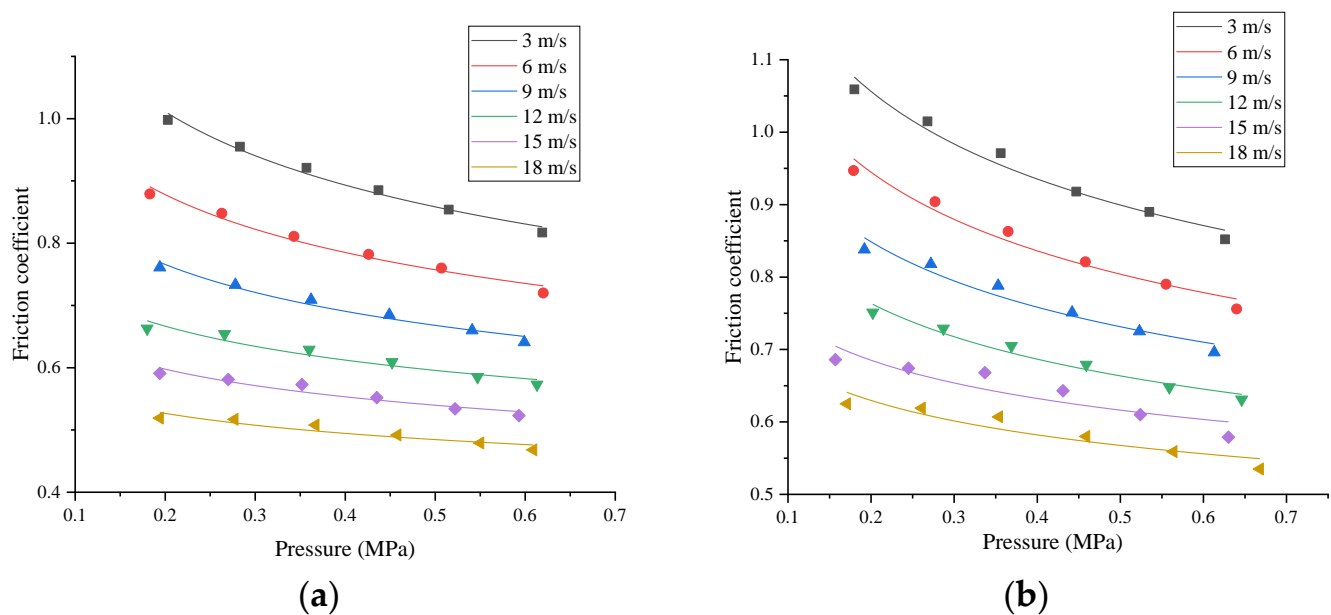| Result Parameters	α_0	α_1	α_2	β_0	β_1	β_2	γ_0	γ_1	γ_2
Rubber A–Road A	0.1872	0.0831	0.0345	1.3352	−0.9469	0.5008	0.0683	−0.0505	0.0732
Rubber A–Road B	0.2793	0.2678	−0.1785	1.357	−0.9318	0.4736	0.0634	−0.0418	0.0826

Figure 13. Fitting curves of wet friction coefficients: (**a**) rubber A in contact with road A; (**b**) rubber A in contact with road B.

3. Simulation Model of Tyre Skid Resistance

3.1. Tyre Model

A passenger car tyre 205/55R16 AU 01 with a complex tread pattern was selected as the research object: firstly, the model of the tread pattern and the carcass components were constructed separately in Hypermesh software; then, the tie command in Abaqus software was used to complete the matching of the single-pitch pattern with the carcass components; thereafter, symmetric model generation was used to generate the 3D model (Figure 14). In the simulation, the rim and the road were modelled as analytical rigid bodies. The aforementioned extended exponential decay friction model of rubber contact with wet road was selected to represent the friction behaviour at the tyre–road interface. The modelling method is detailed in [38]. A contact footprint test for validating the tyre model was conducted; under a load of 4000 N and an inflation pressure of 240 kPa, the widths of the contact footprint were 161 and 163.8 mm, and the lengths were 147 and 148 mm for the test and simulation, respectively, as illustrated in Figure 15. The differences between the test and simulation results were below 2%, indicating favourable agreement. Thus, the finite element method accurately identified tyre deformations, and could be used for subsequent analyses of tyre wet skid resistance.
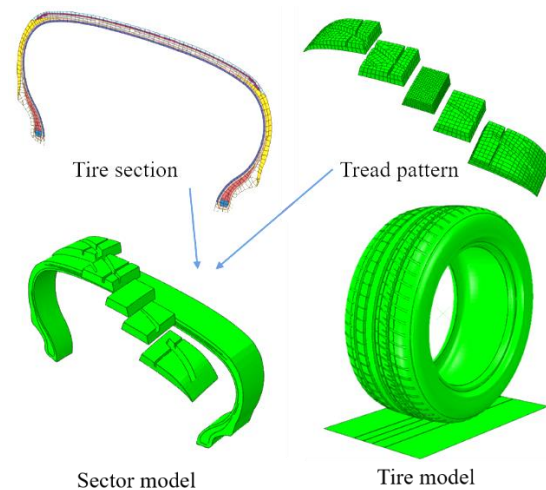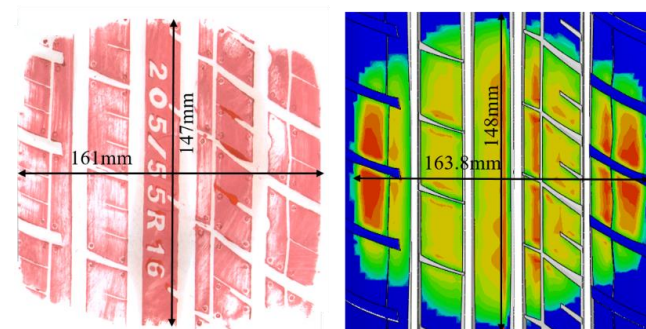

Figure 14. Tyre finite element model.

Figure 15. Parameters of tyre contact footprint.

3.2. Simulation Model of Tyre Wet Skid Resistance

After the loaded tyre reached a stationary rolling condition under a constant travelling speed in the Abaqus Standard solver, the rolling tyre was imported to a non-stationary fluid–structure interaction model for wet skid analysis in the Abaqus Explicit solver. The tyre wet skid simulation was conducted with respect to a moving reference frame, in which the water and road surface were moving toward the rolling tyre at a given speed, and the tyre rolled to a fixed location at a given angular velocity.

Modern automobiles are equipped with anti-braking systems (ABSs) to prevent a rolling tyre from locking up and skidding on the road. The main function of ABS is to control the wheel slip ratio for reaching the maximum braking force. According to a previous study [11], the braking force can be maximised by a peak wheel slip ratio of approximately 18%. In this study, ABS functionality was realised by changing the angular velocity, and the translation velocity of the rolling tyre reached a peak slip ratio of 18%. The slip ratio is defined as follows:

$$S = \frac{v - r_{kc}\omega}{v} \times 100\%$$

(18)

where r_{kc} is the tyre rolling radius, v is the sliding speed, and ω is the tyre rotation angular velocity.

The tyre wet skid simulation model was resolved using the coupled Eulerian–Lagrangian (CEL) method to capture the motion of water. In the CEL method, the flow of the water and the behaviour of the tyre are subjected to Eulerian analysis and traditional nonlinear Lagrangian analysis, respectively. In the CEL method, the material is tracked as it flows through the mesh: this is done by computing its Eulerian volume fraction within each element. The volume fraction $F(x, t)$ of the water was selected to track the water movement zone and boundary, which is expressed in Equation (19):

$$\frac{\partial F}{\partial t} + V \cdot \nabla F = 0$$

(19)

By definition, the element is fully filled with water, and has no water, when $F = 1$ and $F = 0$, respectively. When the sum of all the material volume fractions in an element is <1, (i.e., $0 < F < 1$), the air void will automatically fill the remainder of the element. In the analysis, water flow was treated as that of an incompressible, isotropic, and Newtonian fluid with a constant viscosity. The water temperature and its effects on the tyre were disregarded. In the simulation model, the Eulerian element EC3D8R was used to describe the properties of the water and air.

To enlarge the water flow zone, and to capture the water spray around the tyre sidewall, the sizes of the fluid domain had to be large enough to enclose the region in which the tyre was in contact with the road. In the simulations, the fluid domain had a length of 320 mm and a width of 300 mm, the water depth was 1.5 mm, and the air depth was 298.5 mm (Figure 16). As per the method for measuring the relative wet grip performance of passenger car tyres (GB/T 21910-2008), two tyres 205/55R16 with different tread patterns were used to analyse tyre wet skid resistance: these two tyres were named Tyre AU 01 and Tyre AH 01 (Figure 17). The boundary conditions were as follows: tyre vertical load = 4000 N and tyre air pressure = 240 kPa.
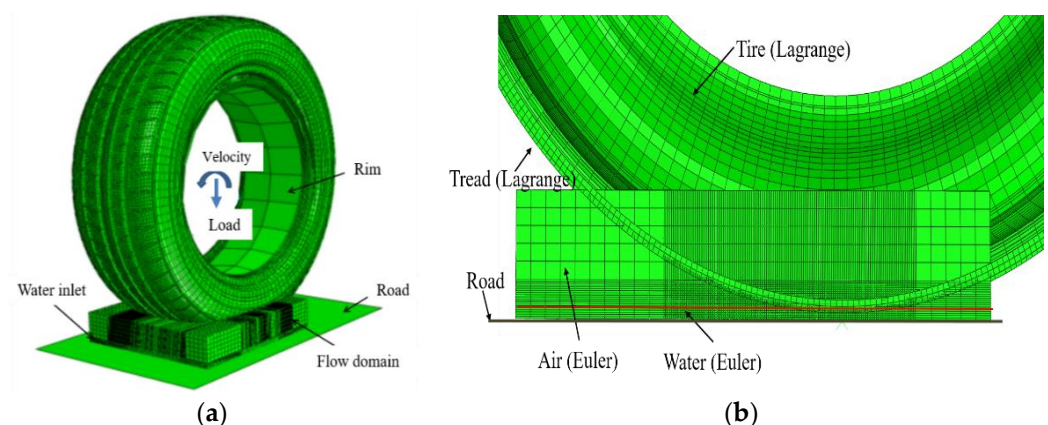

(a)　　　　　　　　　　　　　　　　　　　(b)

Figure 16. Tyre wet road fluid–solid coupling model: (**a**) simulation model; (**b**) partial enlarged view.

Figure 17. Two different test tyres: (**a**) Tyre AU01; (**b**) Tyre AH01.

3.3. Simulation Results Analysis and Verification

3.3.1. Results Analysis

Figure 18 presents the water distribution in the tyre contact regions on road A, with an initial braking speed of 80 km/h: it can be seen that the water flow was smoothly discharged along the tread groove after impacting the tyre. The water flow mark clearly shows that the drainage effect of the tyre grooves was significant; however, because the water film was relatively thin, the generated hydrodynamic lift was too small to lift up the tyre, and most of the tyre tread stayed in contact with road. The tyre front edge was separated from the contact patch by the water impact, and the remaining water around the front edge generated lift, which decreased the tyre contact area.
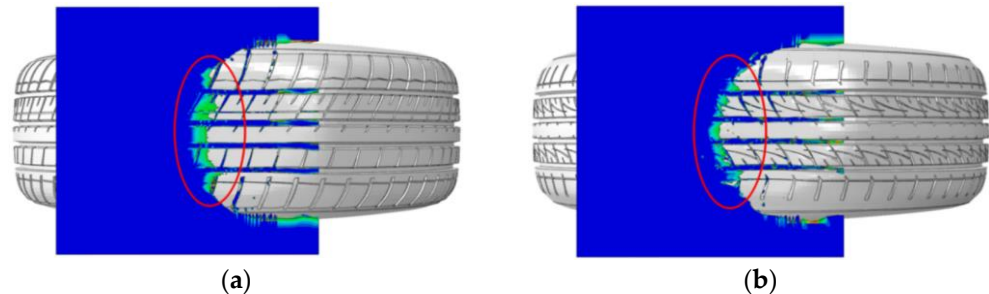

Figure 18. Water distribution between tyre and road surface on wet road surface: (**a**) Tyre AU01 (**b**) Tyre AH01.

As illustrated in Figure 19, the frictional force decreased with the tyre initial braking speed increase for tyres AU 01 and AH 01: this was primarily because the hydrodynamic lift from the water flume increased with the initial braking speed, which weakened the tyre grip on the wet road, and thus decreased the frictional force. Furthermore, the extended-decay friction model proposed was that the friction coefficient decreased with sliding speed, because these two tyres had the same structure design expert for the tread pattern shapes. The frictional forces for these two tyres were approximately equal at low speeds, but the frictional force for AH01 exhibited a larger decrease for every unit increase in speed compared to that of AU01. In general, compared with tyre AU01, tyre AH01 had higher friction at higher speeds, and thus superior wet skid resistance performance.

3.3.2. Experimental Test of Simulation Model

A brake test was conducted on wet road in Yangchen Auto Testing Field in Anhui province, according to the Chinese Government's GB/T 21910-2008 test standards, titled 'Test Method for Relative Gripping Performance of Car Tyre on Wet Pavement'. The test road had a uniform texture and a slope of less than 2%, and the thickness of the water

film on the road was set to 1.5 mm (Figure 20). When the test vehicle reached 80 km/h on the wet road, the driver fully depressed the brake pedal until the vehicle came to a stop. These brake tests were conducted three times by the same driver with the same vehicle, and the mean braking distance (for each set of tyres) was used for analysis. Tyre AH 01 had a shorter braking distance, and thus a larger frictional force, than tyre AU01 (Table 7). The frictional force also varied with the tyre rolling speed. In general, the test results agreed well with their simulation results (illustrated in Figure 19), indicating the accuracy of our simulation method.
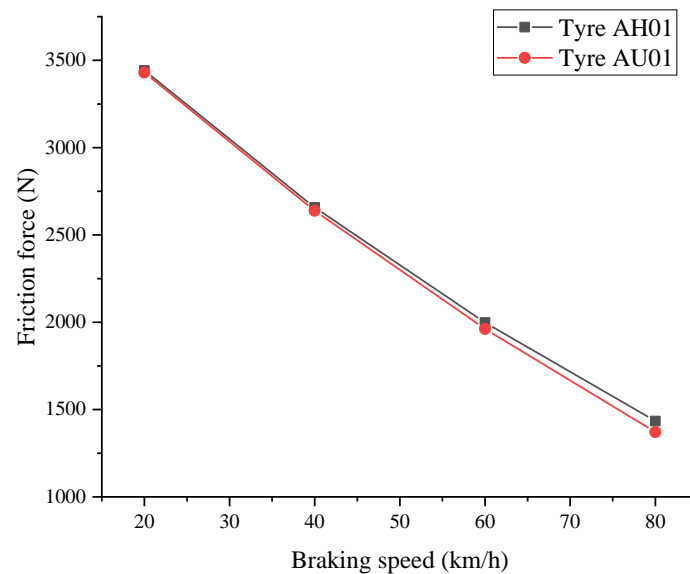

Figure 19. Frictional forces for the two different tyres.

Figure 20. Wet skid braking test.

Table 7. Wet braking test results.

Vehicle Braking Initial Speed 80 Km/h		
Braking distance/m	Tyre AU01	58.3
	Tyre AH01	56.3

4. Analysis of Factors Influencing Tyre Friction

4.1. Influence of Road Roughness

The influence of pavement roughness on tyre wet grip performance was analysed, using roads A and B (described in Section 2.2.3). Road A was smoother and of higher quality than Road B. The friction models for roads A and B employed the parameters indicated in Table 6, which shows the frictional force of tyre AU01 on both roads, A and B, at a tyre load of 3900 N, tyre inflation pressure of 0.24 MPa, and water film thickness of 1.5 mm at the initial braking speeds of 20, 40, 60, and 80 km/h. As depicted in Figure 21, the tyre frictional forces on both road surfaces were lower at higher initial braking speeds, and road B provided higher tyre friction at the same given initial braking speed: this was primarily because the rougher texture of road B resulted in a larger hysteresis friction. Thus, the rougher roads yielded higher wet skid resistance, which maximised driving safety.
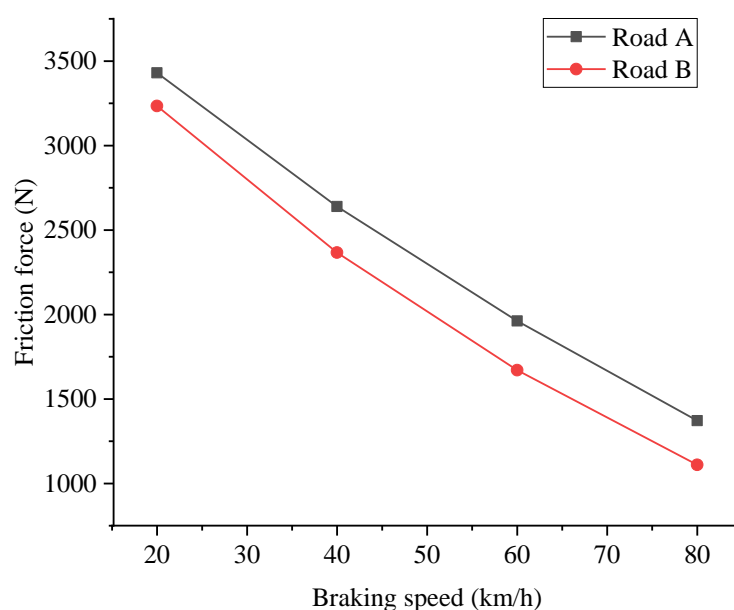

Figure 21. Frictional force on roads A and B.

4.2. Influence of Tyre Characteristics

The influence of tread compound on grip performance was analysed using tyre AU01 with two tread patterns—A and B. According to a previous study [39], tyres with softer treads grip better on dry roads. The rubber features of tyre AU01 are described in Table 2; rubber A was relatively softer than that of rubber B. The tests were conducted at a tyre load of 3900 N, inflation pressure of 0.24 MPa, and water film thickness of 1.5 mm. As indicated in Figure 22, tread A had a greater frictional force than tread B at tyre rolling speeds less than 60 km/h. This was primarily because tread A was softer, resulting in a greater contact area between the tyre and the road, and thus more uniform contact pressure distribution to generate a bigger friction force; however, this difference became smaller at higher rolling speeds, where tread B had a greater frictional force instead. This was primarily because at higher rolling speeds, increasing the hardness of tread B could improve the tread pattern stiffness, enabling it to puncture water film: this resulted in an increased local contact area between the rubber and the road, and thus greater hysteresis friction. In general, a softer tyre tread has better skid performance (and a shorter braking distance) on wet roads.
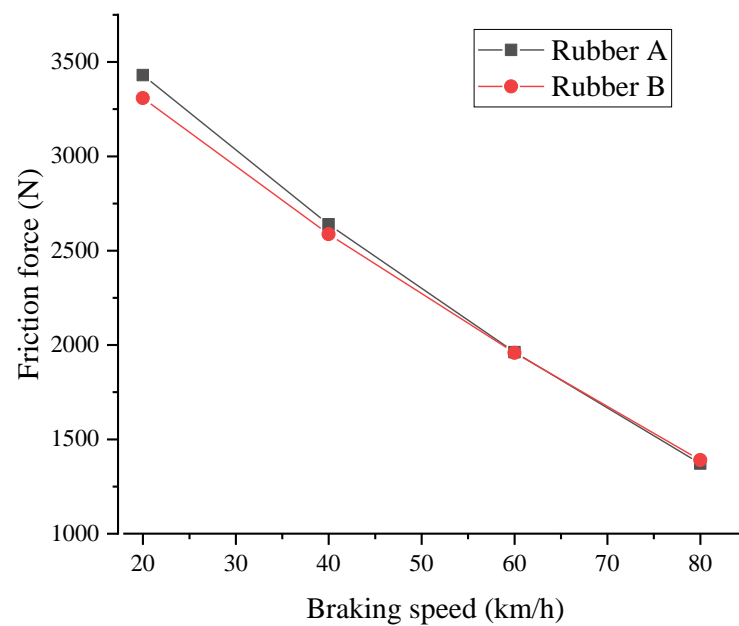
Figure 22. Frictional force under different tread types.

The influences of braking velocity under different loads and the same conditions—tyre air pressure = 0.24 MPa and water film thickness = 1.5 mm—were also analysed. The results indicated that the friction coefficient decreased with the increasing of the initial braking velocity (Figure 23). This trend was due to differences in the contact between the tyre and the road: specifically, an increased initial braking velocity entails greater hydrodynamic lift from water, which reduces the friction coefficient; a greater load results in greater friction because it expands the contact area by increasing tyre deformation. At an initial braking velocity of 80 km/h, the water hydrodynamic lift forces were 1307, 1409, and 1560 N at the tyre loads of 2900, 3900, and 4900 N, respectively: these resulted in a 45%, 36%, and 32% lower vertical contact force between the tyre and the road, respectively. The results also indicated that this decrease in friction with tyre load was slighter at higher braking velocities, which is consistent with the results presented in Reference [40].
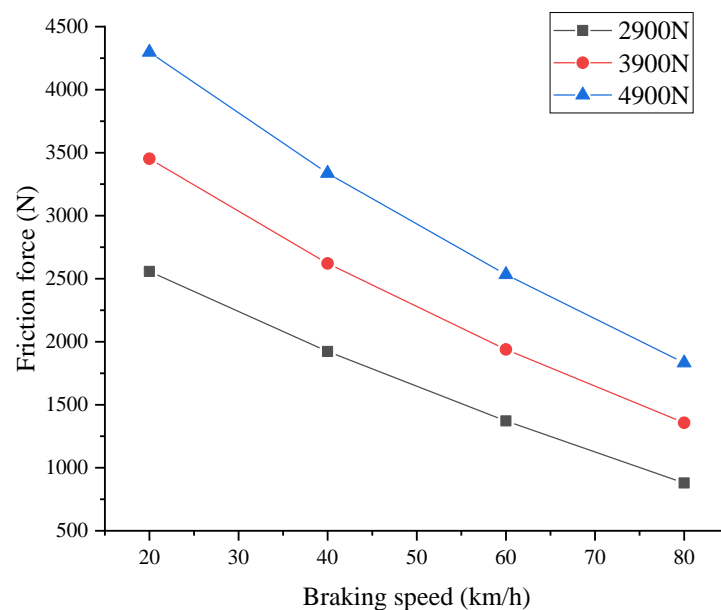

Figure 23. Frictional force under different tyre loads.

The influence of tyre inflation pressure on tyre friction was also analysed. Under the same conditions of tyre load—4900 N and water film thickness = 1.5 mm—the tyre friction force for tyre AU01 decreased as the tyre inflation pressure increased at low braking velocities (Figure 24). It can be seen that friction force decreased as tyre air pressure increased in the lower velocity range, and increased in the higher velocity range, which means that tyre wet skid resistance cannot be predicted easily using tyre air pressure: the main reason for this is that a lower-pressure tyre deforms more easily, and encounters a greater contact area, while the water sealing effect is not obvious, and the hydrodynamic lift force is small. Conversely, the water sealing effect on rough road is greater at higher speeds, the higher hydrodynamic lift force offsets the change of contact area, and a lower tyre pressure results in less friction force. We can speculate that tyre inflation pressure (when not too high, and not too low) most likely is of more value for providing a relatively stable friction performance.
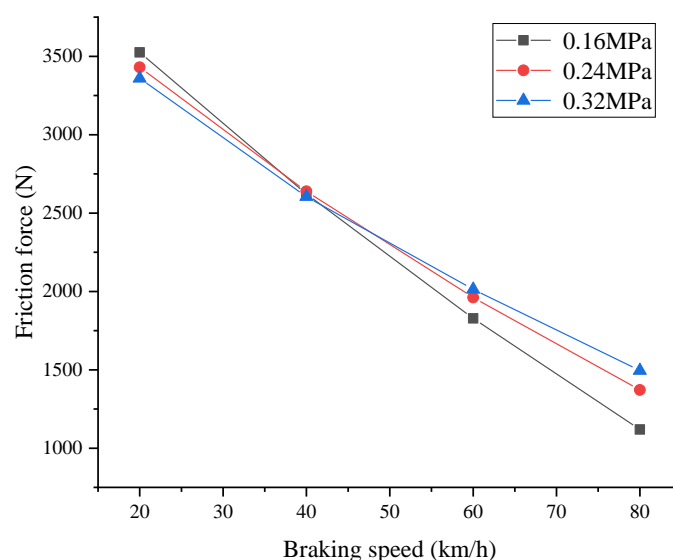

Figure 24. Frictional force under different tyre air pressures.

5. Conclusions

(1) A power spectrum density function was used to describe the topography of the road surface, and the 3D surface of a rough road was reconstructed using the harmonic superposition method. A contact model of the tyre–road interface was established, and the water flume volume when the tyre was sliding on a rough road surface was calculated. The sealing effect of the water film was modelled in terms of the pseudo-hydrodynamic bearing. The contact pressure, hysteresis friction, and water film hydrodynamic lift force were obtained using ABAQUS and Fluent software. These results were used to calculate the friction coefficient, and to establish the extended exponential decay friction model. The results indicate that the friction coefficient decreases gradually with pressure and sliding speed, that the magnitude of the decline increases with the increase of the sliding speed, and that the proposed friction model has enough accuracy to support the numerical simulation of tyre wet skid resistance on a wet rough road.

(2) A finite element model was established using ABAQUS software, and was verified using a static contact pressure test. A simulation model of tyre wet grip performance was established using the CEL method, and the proposed extended exponential decay friction model was applied to the simulation model, to describe the characteristics of the tyre–road interface. To validate the simulation model, two tyres were compared, in terms of braking distance. The simulation results indicate that a rougher pavement provides better wet skid resistance. When a thin water film is present, a softer tyre

rubber has a larger contact area with the road, and thus higher wet friction. For tyre wet grip in general, at a high braking speed, a higher vertical load results in greater wet grip performance. Tyre air pressure should be kept at the recommended value, to maintain a relatively stable wet friction force, which ensures safety at different speeds.

Author Contributions: Conceptualisation, L.Z.; methodology, L.Z., R.W. and H.Z.; supervision, G.W.; writing—original draft, L.Z.; writing—review and editing, L.Z. and R.W. All authors have read and agreed to the published version of the manuscript.

Data Availability Statement: Not applicable.

Conflicts of Interest: The authors declare no conflict of interest.

References

1. Maleska, M.; Petry, F.; Fehr, D.; Schuhmann, W.; Böhle, M. Longitudinal hydroplaning performance of passenger car tyres. *Veh. Syst. Dyn.* **2021**, *59*, 415–432. [CrossRef]
2. Bai, X.; Chen, G.; Li, W.; Jia, R.; Xuan, L.; Zhu, A.; Wang, J. Critical Speeds of Electric Vehicles for Regenerative Braking. *Automot. Innov.* **2021**, *4*, 201–214. [CrossRef]
3. Kane, M.; Do, M.T.; Cerezo, V.; Rado, Z.; Khelifi, C. Contribution to pavement friction modelling: An introduction of the wetting effect. *Int. J. Pavement Eng.* **2019**, *20*, 965–976. [CrossRef]
4. Wu, J.; Zhang, C.; Wang, Y.; Su, B.; Gond, B. Investigation on wet skid resistance of tread rubber. *Exp. Tech.* **2019**, *43*, 81–89. [CrossRef]
5. Ueckermann, A.; Wang, D.; Oeser, M.; Steinauer, B. Calculation of skid resistance from texture measurements. *J. Traffic Transp. Eng.* **2015**, *2*, 3–16. [CrossRef]
6. US Department of Transportation; Federal Highway Administration. How Do Weather Events Impact Roads? 2019. Available online: https://ops.fhwa.dot.gov/weather/q1_roadimpact.htm (accessed on 1 May 2019).
7. Fuentes, L.; Gunaratne, M.; Hess, D. Evaluation of the effect of pavement roughness on skid resistance. *J. Transp. Eng.* **2010**, *136*, 640–653. [CrossRef]
8. Anupam, K.; Tang, T.; Kasbergen, C.; Scarpas, A.; Erkens, S. 3-D Thermomechanical Tyre–Pavement Interaction Model for Evaluation of Pavement Skid Resistance. *Transp. Res. Rec.* **2021**, *2675*, 65–80. [CrossRef]
9. Xu, N.; Yang, Y.; Guo, K. A Discrete Tyre Model for Cornering Properties Considering Rubber Friction. *Automot. Innov.* **2020**, *3*, 133–146. [CrossRef]
10. Serigos, P.A.; De Fortier Smit, A.; Prozzi, J.A. Incorporating surface microtexture in the prediction of skid resistance of flexible pavements. *Transp. Res. Rec.* **2014**, *2457*, 105–113. [CrossRef]
11. Li, J.; Song, Z.; Wei, Y.; Ouyangm, M. Influence of tire dynamics on slip ratio estimation of independent driving wheel system. *Chin. J. Mech. Eng.* **2014**, *27*, 1203–1210. [CrossRef]
12. Khasawneh, M.; Liang, R.Y. Air void effects on frictional properties of existing asphalt pavement surfaces. *Int. J. Pavements* **2011**, *10*, 62–71.
13. Persson, B.N.J.; Tartaglino, U.; Albohr, O.; Tosatti, E. Rubber friction on wet and dry road surfaces: The sealing effect. *Phys. Rev. B* **2005**, *71*, 035428. [CrossRef]
14. Yin, Y.; Wen, H.; Sun, L.; Hou, W. The influence of road geometry on vehicle rollover and skidding. *Int. J. Environ. Res. Public Health* **2020**, *17*, 1648. [CrossRef] [PubMed]
15. Sabey, E.B. Pressure Distributions beneath Spherical and Conical Shapes pressed into a Rubber Plane, and their Bearing on Coefficients of Friction under Wet Conditions. *Proc. Phys. Soc.* **1958**, *71*, 979–988. [CrossRef]
16. Grosch, K.A. The Relation between the Friction and ViscoElastic Properties of Rubber. *Proc. R. Soc. A* **1963**, *274*, 21–39. [CrossRef]
17. Takino, H.; Nakayama, R.; Yamada, Y.; Kohjiya, S.; Matsuo, T. Viscoelastic properties of elastomers and tyre wet skid resistance. *Rubber Chem. Technol.* **1997**, *70*, 584–594. [CrossRef]
18. Deleau, F.; Mazuyer, D.; Koenen, A. Sliding friction at elastomer/glass contact: Influence of the wetting conditions and instability analysis. *Tribol. Int.* **2009**, *42*, 149–159. [CrossRef]
19. Zhao, H.; Wu, M.; Wu, S. Variation of asphalt pavement friction coefficient with change of water film thickness. *J. Civ. Aviat. Univ. China* **2015**, *33*, 47–52.
20. Greenwood, J.A.; Tabor, D. The Friction of Hard Sliders on Lubricated Rubber: The Importance of Deformation Losses. *Proc. Phys. Soc.* **1960**, *71*, 989. [CrossRef]
21. Greenwood, J.A.; Minshall, H.; Tabor, D. Hysteresis Losses in Rolling and Sliding Friction. *Proc. R. Soc. A Math. Phys. Eng. Sci.* **1961**, *259*, 480–507.
22. Persson, B.N.J.; Tartaglino, U.; Albohr, O.; Tosatti, E. Sealing is at the origin of rubber slipping on wet roads. *Nat. Mater.* **2004**, *3*, 882–885. [CrossRef] [PubMed]

23. Ji, T.; Huang, X.; Liu, Q. Part hydroplaning effect on pavement friciton coefficient. *J. Traffic Transp. Eng.* **2003**, *3*, 10–12.
24. Scaraggi, M.; Angerhausen, J.; Dorogin, L.; Murrenhoff, H.; Persson, B. Influence of anisotropic surface roughness on lubricated rubber friction: Extended theory and an application to hydraulic seals. *Wear* **2017**, *410–411*, 43–62. [CrossRef]
25. Peng, J.; Chu, L.; Fwa, T.F. Determination of safe vehicle speeds on wet horizontal pavement curves. *Road Mater. Pavement Des.* **2021**, *22*, 2641–2653. [CrossRef]
26. Ding, Y.; Wang, H. Evaluation of hydroplaning risk on permeable friction course using tyre–water–pavement interaction model. *Transp. Res. Rec.* **2018**, *2672*, 408–417. [CrossRef]
27. Tang, T.; Anupam, K.; Kasbergen, C.; Scarpas, A.; Erkens, S. A finite element study of rain intensity on skid resistance for permeable asphalt concrete mixes. *Constr. Build. Mater.* **2019**, *220*, 464–475. [CrossRef]
28. Huang, X.; Cao, Q.; Liu, X.; Wang, H.; Chen, J. Simulation of vehicle braking performance on rainy dyas based on pavement surface fractal friciton theory. *J. Jilin Univ. (Eng. Technol. Ed.)* **2019**, *49*, 757–765.
29. Heinrich, G.; Klüppel, M. Rubber friction, tread deformation and tyre traction. *Wear* **2008**, *265*, 1052–1060. [CrossRef]
30. Yang, Y.; Zhu, X.; Jelagin, D.; Guarin, A.; Steyn, W.J. Numerical analysis concerning the skid resistance of rubber-contaminated runway grooves. *Tribol. Int.* **2021**, *163*, 107157. [CrossRef]
31. Kumar, A.; Gupta, A. Review of Factors Controlling Skid Resistance at Tyre-Pavement Interface. *Adv. Civ. Eng.* **2021**, *2021*, 2733054.
32. Li, P.; Feng, G.; Deng, X. Three-dimensional virtual road's harmonic reconstruction. *Automot. Eng.* **2014**, *11*, 24–27.
33. Wang, G.; Ma, Y.; Liang, C.; Wan, Z. Locust's pads bionic structural design of radial tyre crown. *J. Mech. Eng.* **2013**, *49*, 131–135. [CrossRef]
34. Wang, G.; Fu, J.; Zhou, H.; Yang, J.; Liang, C. Tyre Grip Performance Simulation and Improving Method Considering the Influence of Tread Pattern Stiffness. *J. Donghua Univ. (Engl. Ed.)* **2016**, *33*, 939–943.
35. Zhou, H.; Li, H.; Liang, C.; Zhang, L.; Wang, G. Relationship between Tyre Ground Characteristics and Vibration Noise. *Stroj. Vestn. J. Mech. Eng.* **2021**, *67*, 11–27. [CrossRef]
36. Jayme, A.; Al-Qadi, I.L. Thermomechanical coupling of a hyper-viscoelastic truck tyre and a pavement layer and its Impact on three-dimensional contact stresses. *Transp. Res. Rec.* **2021**, *2675*, 359–372. [CrossRef]
37. Oden, J.T.; Martins, J.A.C. Models and computational methods for dynamic friction phenomena. *Comput. Methods Appl. Mech. Eng.* **1985**, *52*, 527–634. [CrossRef]
38. Zhou, H.; Wang, G.; Yang, J.; Xue, K. Numerical Simulation of the Effect of Bionic V-riblet Non-smooth Surface on Tyre Anti-hydroplaning. *J. Cent. South Univ.* **2015**, *22*, 3900–3908. [CrossRef]
39. Pongdhorn, S.O.; Krisda, S.; Chakrit, S.; Wenussarin, I.; Pram, Y.; Uthai, T. Effects of Blend Ratio and SBR Type on Properties of Carbon Black-Filled and Silica-Filled SBR/BR Tyre Tread Compounds. *Adv. Mater. Sci. Eng.* **2017**, *2017*, 2476101.
40. Ong, G.P.; Fwa, T.F. Modeling skid resistance of commercial trucks on highways. *J. Transp. Eng.* **2019**, *136*, 510–517. [CrossRef]